Showcasing research from Dr. Hajime Suzuki's group in Prof. Ryu Abe's laboratory, Graduate School of Engineering, Kyoto University, Japan.

Vanadium-based oxyhalide photocatalysts for visible-light-driven Z-scheme water splitting: advancing conduction band engineering

This study demonstrates the potential of V-based oxyhalides as oxygen-evolving photocatalysts in Z-scheme water-splitting systems. Owing to the positively located conduction band derived from vanadium orbitals, $PbVO_3Cl$ absorbs visible light up to 550 nm and functions as an oxygen-evolving photocatalyst under visible light irradiation.

Image reproduced by permission of Ryu Abe from *J. Mater. Chem. A*, 2025, **13**, 25356.

As featured in:

See Hajime Suzuki, Ryu Abe *et al.*, *J. Mater. Chem. A*, 2025, **13**, 25356.

ROYAL SOCIETY OF CHEMISTRY

rsc.li/materials-a

PAPER

Check for updates

Vanadium-based oxyhalide photocatalysts for visible-light-driven Z-scheme water splitting: advancing conduction band engineering†

Hajime Suzuki, [ID] *[a] Ryuki Tomita,[a] Yusuke Ishii, [ID] [a] Osamu Tomita, [ID] [a] Akinobu Nakada, [ID] [ab] Akinori Saeki [ID] [c] and Ryu Abe [ID] *[a]

Z-scheme water-splitting systems have garnered significant attention as a promising technology for producing hydrogen cleanly from water using solar energy. Layered oxyhalides have emerged as efficient oxygen-evolving photocatalysts (OEPs) for these systems. However, the conduction band minimum (CBM) of these oxyhalides is excessively negative compared to the reduction potential of electron mediators. This limitation underscores the need for novel conduction band engineering approaches to narrow the band gap and enable the utilization of visible light across a broader spectrum. This study introduces vanadium-based oxyhalides as OEPs in the Z-scheme system. The physicochemical properties and photocatalytic activities of three lead-vanadium-based oxyhalides, $Pb_{14}(VO_4)_2O_9Cl_4$, $Pb_5(VO_4)_3Cl$, and $PbVO_3Cl$, were comprehensively characterized. The CBMs of these materials were found to be more positive than those of conventional oxyhalide photocatalysts and displayed significant variation. $PbVO_3Cl$ exhibited the most positive CBM and the smallest band gap, enabling visible light absorption up to approximately 550 nm. Madelung site potential analysis of each vanadium cation highlighted the reasons for the significant difference in CBM positions among the Pb–V oxyhalides. Remarkably, $PbVO_3Cl$ exhibited oxygen evolution activity under visible light irradiation, marking the first instance of a vanadium-based oxyhalide as an OEP in a Z-scheme system. This exceptional activity of $PbVO_3Cl$ was attributed to the superior carrier transport properties, owing to the interconnected VO_5 units, as revealed by time-resolved microwave conductivity (TRMC) measurements, as well as the extended visible light absorption.

Introduction

Water splitting using semiconductor photocatalysts has gained significant attention as a promising technology for producing hydrogen cleanly from water by harvesting abundant solar energy.[1–8] To achieve practical (*i.e.*, cost-effective) solar-to-hydrogen conversion efficiency, it is essential to efficiently utilize photons in the visible light region rather than just in the UV region. A Z-scheme water-splitting system has demonstrated great potential in capturing a broad range of visible light, and its efficiency has steadily improved in recent years.[9–12] This system typically consists of a mixture of two different photocatalyst particles: a hydrogen-evolving photocatalyst (HEP) and

an oxygen-evolving photocatalyst (OEP), along with a redox couple (Ox/Red), such as Fe^{3+}/Fe^{2+}, dissolved in an aqueous solution. By reducing the energy required to excite each photocatalyst, this system enables the utilization of various visible-light-responsive photocatalysts capable of absorbing light with long wavelengths. In other words, it allows semiconductors with water reduction or oxidation potentials suitable for one side of the system to be effectively employed. For example, visible-light-responsive oxides, such as tungsten trioxide (WO_3), can function as OEPs if they can reduce the oxidant to a reductant.[9] Similarly, non-oxide photocatalysts (*e.g.*, (oxy)sulfides, (oxy)nitrides, and dyes) can act as HEPs if they can oxidize the reductant to an oxidant.[13–18]

Recently, Sillén(-Aurivillius)-type layered oxyhalides such as Bi_4NbO_8Cl and $PbBiO_2Cl$, have emerged as promising OEPs for visible-light-driven Z-scheme water splitting.[19–21] The valence band maximum (VBM) of these oxyhalides is mainly composed of elevated O-2p orbitals, where photogenerated holes are preferentially consumed by water oxidation rather than self-oxidation (halogen oxidation), resulting in their substantially high stabilities as OEPs in Z-scheme water splitting systems.[22,23] The conduction band minimum (CBM) of these oxyhalides is

[a]Department of Energy and Hydrocarbon Chemistry, Graduate School of Engineering, Kyoto University, Katsura, Nishikyo-ku, Kyoto 615-8510, Japan. E-mail: suzuki.hajime.7x @kyoto-u.ac.jp; ryu-abe@scl.kyoto-u.ac.jp

[b]Precursory Research for Embryonic Science and Technology (PRESTO), Japan Science and Technology Agency (JST), 4-1-8 Honcho, Kawaguchi, Saitama 332-0012, Japan

[c]Department of Applied Chemistry, Graduate School of Engineering, Osaka University, 2-1 Yamadaoka, Suita, Osaka 565-0871, Japan
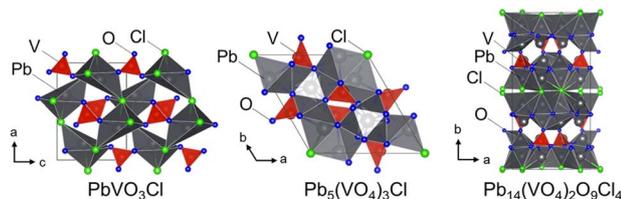
Fig. 1 Crystal structures of Pb–V-based oxyhalides: PbVO$_3$Cl, Pb$_5$(VO$_4$)$_3$Cl, and Pb$_{14}$(VO$_4$)$_2$O$_9$Cl$_4$.

primarily composed of Bi-6p or Pb-6p orbitals and is sufficiently negative relative to the water reduction potential, enabling them to evolve hydrogen (H$_2$) from water under light irradiation.[19,24–27] However, such negative CBMs are not required when these materials are employed as OEPs in Z-scheme systems with redox mediators. In an ideal OEP in Z-scheme systems, the CBM should be somewhat more negative than the reduction potential of electron mediators. However, the CBM of the above oxyhalides (e.g., Bi$_4$NbO$_8$Cl) is excessively negative. This motivates the development of oxyhalides with CBMs positioned at more positive potentials, resulting in narrower bandgaps for harvesting photons in longer wavelength regions.

This study focused on pentavalent vanadium(v) cations. The V cation with high ionization energy is expected to form CBMs at more positive potentials. After exploring various Pb(Bi)–V-based oxyhalides, PbVO$_3$Cl, Pb$_5$(VO$_4$)$_3$Cl, and Pb$_{14}$(VO$_4$)$_2$O$_9$Cl$_4$ (Fig. 1) were selected.[28–30] Their optical properties, band structures, and photocatalytic activities were evaluated, and their relationships were investigated through various experimental and theoretical investigations.

Experimental

Materials

Lead(II) oxide (PbO, 99.5%), vanadium(v) oxide (V$_2$O$_5$, 99.0%), sodium metavanadate(v) (NaVO$_3$, 99.5%), boric acid (B(OH)$_3$, 99.5%), sodium orthovanadate(v) (Na$_3$VO$_4$, 99.98%), sodium chloride (NaCl, 99.5%), lead(II) nitride (Pb(NO$_3$)$_2$, 99.9%), disodium hydrogenphosphate 12-water (Na$_2$HPO$_4$·12H$_2$O, 99%), sodium dihydrogenphosphate 2-water (NaH$_2$PO$_4$·2H$_2$O, 99%), iron(III) chloride hexahydrate (FeCl$_3$·6H$_2$O, 99%), iron(III) nitrate nonahydrate (Fe(NO$_3$)$_3$·9H$_2$O, 99%), iron(III) perchlorate n-hydrate (Fe(ClO$_4$)$_3$, 70% as anhydrous), iron(III) sulfate n-hydrate (Fe$_2$(SO$_4$)$_3$, 60–80% as anhydrous), nitric acid (HNO$_3$, 69% as assay), perchloric acid (HClO$_4$, 70% as assay), hydrochloric acid (HCl, 35% as assay), sulfuric acid (H$_2$SO$_4$, 95% as assay), and ruthenium chloride n-hydrate (RuCl$_3$·nH$_2$O, 99.9%) were purchased from FUJIFILM Wako Chemicals. Lead(II) chloride (PbCl$_2$, 99.999%) and sodium orthovanadate(v) (Na$_3$VO$_4$, 99.98%) were purchased from Sigma-Aldrich. Ammonium vanadate(v) (NH$_4$VO$_3$, 99.0%) was purchased from KANTO CHEMICAL.

Synthesis of PbVO$_3$Cl

PbVO$_3$Cl was synthesized using solid-state and hydrothermal methods, following previously reported procedures.[28,31] In the solid-state method, PbO, PbCl$_2$, and V$_2$O$_5$ were used as starting materials, with masses of 0.37 g (1.65 mmol), 0.46 g (1.65 mmol), and 0.30 g (1.65 mmol), respectively. These components were mixed thoroughly for 15 minutes, pelletized, and sealed in a vacuum quartz tube. The sample was then calcined at 450 °C for 24 hours with heating and cooling rates of 3 °C min^{-1} to yield the desired product. For the hydrothermal method, PbCl$_2$, NaVO$_3$, and B(OH)$_3$ were employed as raw materials, with masses of 3.7 g (13.2 mmol), 1.6 g (13.2 mmol), and 3.8 g (61.2 mmol), respectively. These reagents were added to 36 mL of deionized water, stirred, and transferred into a 100 mL Teflon-lined autoclave. The mixture was heated at 170 °C for 24 hours. The resulting product was washed with deionized water and dried overnight at 60 °C in a drying oven. The X-ray diffraction (XRD) patterns of the obtained samples are shown in Fig. S1.† The sample synthesized via the solid-state method contained impurities, including PbCl$_2$ and Pb$_5$(VO$_4$)$_3$Cl, whereas the hydrothermally synthesized sample was free of impurities. X-ray photoelectron spectroscopy (XPS) measurements were also performed for the hydrothermally synthesized sample, confirming the presence of the expected elements at the surface, predominantly in their intended oxidation states (Fig. S2†). Therefore, the hydrothermally synthesized sample was used for all investigations.

Synthesis of Pb$_5$(VO$_4$)$_3$Cl

Pb$_5$(VO$_4$)$_3$Cl was synthesized via a precipitation method based on a procedure reported previously.[32] Specifically, 0.55 g (3 mmol) of Na$_3$VO$_4$ and 0.058 g (1 mmol) of NaCl were dissolved in 50 mL of deionized water. To this solution, an aqueous solution containing 1.7 g (5 mmol) of Pb(NO$_3$)$_2$ dissolved in 50 mL of deionized water was slowly added dropwise. The resulting suspension was stirred for 1 hour, washed with deionized water, and dried overnight at 60 °C in a drying oven to obtain Pb$_5$(VO$_4$)$_3$Cl (Fig. S3†).

Synthesis of Pb$_{14}$(VO$_4$)$_2$O$_9$Cl$_4$

Pb$_{14}$(VO$_4$)$_2$O$_9$Cl$_4$ was synthesized via a solid-state reaction. PbO, PbCl$_2$, and V$_2$O$_5$ were weighed precisely at 0.88 g (3.96 mmol), 0.18 g (0.66 mmol), and 0.060 g (0.33 mmol), respectively. These materials were mixed thoroughly for 15 minutes and then pelletized. The pellets were sealed in a vacuum quartz tube and subjected to heat treatment at 300–700 °C for 24 hours, with heating and cooling rates of 3 °C min^{-1}.

Electrochemical measurement

Mott–Schottky plots were recorded in a three-electrode electrochemical cell equipped with a platinum (Pt) wire counter-electrode and Ag/AgCl reference electrode in a phosphate-buffered solution (0.1 M, pH 6.0). Measurements were performed using an electrochemical analyzer (VersaSTAT 4, Princeton Applied Research) with an amplitude of 10 mV and a frequency of 1000 Hz. The Mott–Schottky plots for the V-based oxyhalides were obtained in the stable potential range determined from cyclic voltammetry measurements. The electrode was prepared using the squeegee method. A particulate sample

This journal is © The Royal Society of Chemistry 2025

J. Mater. Chem. A, 2025, 13, 25356–25362 | 25357

was mixed with a small amount of water, coated on a fluorine-doped tin oxide (FTO) conductive substrate, and dried overnight at room temperature. The coated area was fixed at *ca.* 1.5 × 4.0 cm^2. Photoelectrochemical measurements were also carried out using the same setup and electrode, under chopped visible light from a 300 W Xe lamp with a cutoff filter (L-42, HOYA).

Characterization

Powder X-ray diffraction (XRD; MiniFlex II, Rigaku, Cu Kα), X-ray photoelectron spectroscopy (XPS; ESCA MT-5500, ULVAC-PHI, Mg Kα), scanning electron microscopy (SEM; NVision 40, Carl Zeiss-SIINT), and ultra-violet (UV)-vis diffuse reflectance spectroscopy (V-650, Jasco) were used to characterize the samples. The collected XRD data were analyzed using Jana2006.[33] The XPS binding energies were corrected with reference to the C 1s peak at 284.8 eV. The VESTA program was used to draw crystal structures and calculate Madelung site potentials.[34] The ionization energy was directly measured by PYS (BIP-KV201, Bunkoukeiki) in a vacuum (<5 × 10^{-2} Pa). Time-resolved microwave conductivity (TRMC) measurements were performed using the third harmonic generation (THG) at 355 nm ($I_0 = 4.6 × 10^{15}$ photons per cm^2 per pulse) from a Nd:YAG laser (Continuum Inc., Surelite II, 5–8 ns pulse duration, 10 Hz) as the excitation source. The resonant frequency and microwave power were set to ~9.1 GHz (X-band) and 3 mW, respectively.

Calculation

The partial density of states (PDOS) was calculated using the Cambridge Serial Total Energy Package (CASTEP).[35] The energy was calculated using the generalized gradient approximation (GGA) of density functional theory (DFT) as proposed by Perdew, Burke, and Ernzerhof (PBE). Electronic states were expanded using a plane-wave basis set with a cutoff value of 630 eV, and the *k*-point meshes were set as 5 × 5 × 5. Geometry optimization was performed before the PDOS calculations using the Broyden–Fletcher–Goldfarb–Shanno (BFGS) algorithm.

Photocatalytic reactions

The loading of the Fe/Ru oxide ((Fe,Ru)O$_x$) cocatalyst was performed by simultaneous impregnation using FeCl$_3$ and RuCl$_3$ precursors corresponding to 0.5 and 0.9 wt% of Fe and Ru, respectively.[36] The photocatalyst powder was dispersed in a portion of an aqueous solution containing FeCl$_3$ and RuCl$_3$, followed by evaporation of the solvent in a water bath with heating at 573 K for 1 h under an argon flow (20 mL min^{-1}). As a HEP in Z-scheme water splitting, rhodium-doped strontium titanate (SrTiO$_3$:Rh)[37] was synthesized by a solid-state reaction. A mixture of TiO$_2$, SrCO$_3$, and Rh$_2$O$_3$, with a molar ratio of Ti : Sr : Rh = 1 : 1.07 : 0.01, was calcined in an alumina crucible at 600 °C for 2 h and subsequently at 1000 °C for 10 h with intermediate grinding. A Ru-based cocatalyst was then deposited on SrTiO$_3$:Rh by a photo-deposition method.[38] SrTiO$_3$:Rh was suspended in a 10 vol% methanol aqueous solution

containing RuCl$_3$ (0.7 wt% as Ru metal) and irradiated with visible light (400 < λ < 800 nm) for 2 h.

Photocatalytic reactions were carried out in a Pyrex glass reactor connected to a closed gas circulation system. For water oxidation with an electron acceptor, the photocatalyst powder (0.1 g) was suspended in 250 mL of an aqueous solution containing Fe(NO$_3$)$_3$, Fe(ClO$_4$)$_3$, FeCl$_3$, or Fe$_2$(SO$_4$)$_3$ (5 mM as Fe) in the reactor. A small amount of aqueous HNO$_3$, HClO$_4$, HCl, or H$_2$SO$_4$ solution was added to the respective aqueous solutions of Fe(NO$_3$)$_3$, Fe(ClO$_4$)$_3$, FeCl$_3$, or Fe$_2$(SO$_4$)$_3$, to adjust the pH to 2.4 before the reaction. For the Z-scheme water-splitting reaction with the Fe^{3+}/Fe^{2+} redox couple, Ru-loaded SrTiO$_3$:Rh (0.1 g) and (Fe,Ru)O$_x$-loaded PbVO$_3$Cl (or unmodified PbVO$_3$Cl) (0.1 g) were suspended together in an aqueous Fe(NO$_3$)$_3$ or Fe(ClO$_4$)$_3$ solution (5 mM, 250 mL) as the HEP and OEP, respectively. The suspensions were irradiated using a 300 W Xe lamp with a cutoff filter (L-42, HOYA) and a cold mirror (CM-1, Kenko) under magnetic stirring. The evolved gases were analyzed by using an online gas chromatograph (Shimadzu, GC-8A, thermal conductivity detector (TCD); 5 Å molecular sieve column packing; Ar carrier gas).

Results and discussion

Synthesis and characterization

PbVO$_3$Cl and Pb$_5$(VO$_4$)$_3$Cl particles were successfully synthesized as single phases using previously reported synthesis methods (Fig. S1 and S3†).[28,32] Although the synthesis of Pb$_{14}$(VO$_4$)$_2$O$_9$Cl$_4$ has not been reported, it is structurally characterized as a mineral.[30] In this study, the synthesis was attempted *via* the conventional solid-state method. The XRD patterns of the synthesized samples are shown in Fig. 2. The XRD patterns of samples calcined at 550 °C and 600 °C are almost identical to the reported patterns. Furthermore, Le Bail analysis yielded good fits for the XRD patterns of both samples (Fig. S4†). These
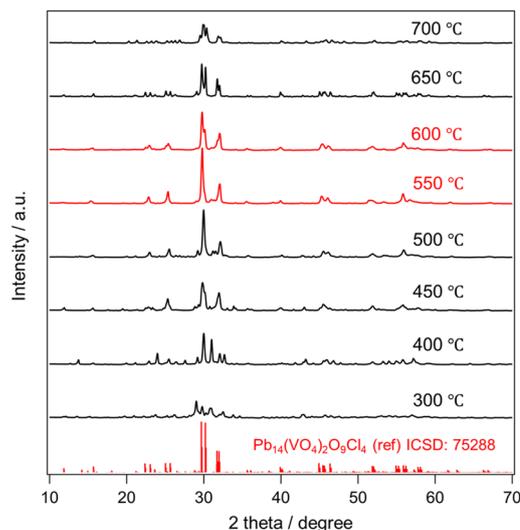

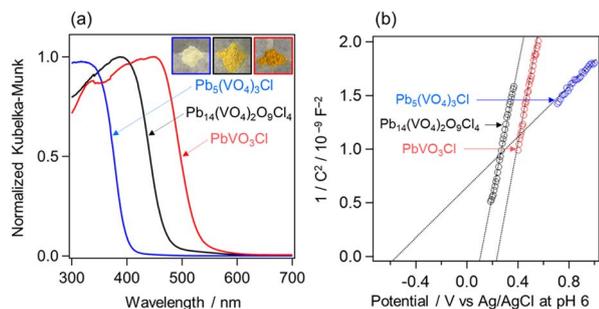**Fig. 2** XRD patterns of the samples synthesized at various temperatures from precursor materials, aiming to synthesize Pb$_{14}$(VO$_4$)$_2$O$_9$Cl$_4$.

25358 | *J. Mater. Chem. A*, 2025, **13**, 25356–25362

This journal is © The Royal Society of Chemistry 2025

Fig. 3 (a) Diffuse reflectance spectra and (b) Mott–Schottky plots of $Pb_5(VO_4)_3Cl$, $Pb_{14}(VO_4)_2O_9Cl_4$, and $PbVO_3Cl$. The inset photographs are physical appearances of the oxyhalides.

results confirm the successful synthesis of $Pb_{14}(VO_4)_2O_9Cl_4$ *via* solid-state synthesis at appropriate temperatures. The sample synthesized at 600 °C was used for further characterization. SEM images of the obtained $PbVO_3Cl$, $Pb_5(VO_4)_3Cl$, and $Pb_{14}(VO_4)_2O_9Cl_4$ shown in Fig. S5† reveal large particles with sizes of several hundred nanometers to several micrometers.

The diffuse reflectance spectra and Mott–Schottky plots for $Pb_5(VO_4)_3Cl$, $Pb_{14}(VO_4)_2O_9Cl_4$, and $PbVO_3Cl$ are shown in Fig. 3. The absorption edges of $Pb_5(VO_4)_3Cl$, $Pb_{14}(VO_4)_2O_9Cl_4$, and $PbVO_3Cl$ are approximately 415, 440, and 550 nm, respectively. The band gaps were estimated from Tauc plots (Fig. S6 and S7†). The flat-band potentials determined from the Mott–Schottky plots (*vs.* Ag/AgCl at pH 6) are −0.58 V, +0.10 V, and +0.23 V for $Pb_5(VO_4)_3Cl$, $Pb_{14}(VO_4)_2O_9Cl_4$, and $PbVO_3Cl$, respectively.

Based on the measurements, the estimated band positions of each Pb–V oxyhalide were compared with those of conventional layered oxyhalide photocatalysts (Fig. 4). The flat band potentials were assumed to be located just below the CBMs due to the n-type nature of these materials. Among the three Pb–V oxyhalides, the CBMs varied significantly, whereas the VBMs were close to each other. Notably, $PbVO_3Cl$ exhibited the most positive CBM, resulting in a narrower bandgap and enabling the broadest absorption in the visible region. Compared to conventional oxyhalide photocatalysts, all the Pb–V oxyhalides displayed more positive CBMs. The validity of this CBM position was further supported by PYS measurement (Fig. S8†).
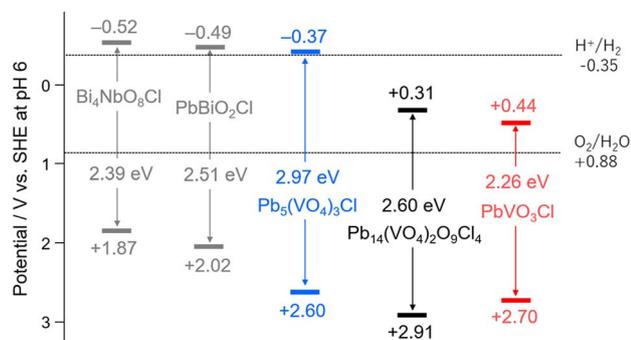
Band structures of Pb–V oxyhalides

The partial density of states (PDOS) calculated using DFT is shown in Fig. 5a–c. In all compounds, the VBM is predominantly composed of O-2p orbitals, with noticeable hybridization with Pb-6s orbitals, similar to what has been observed in other Pb-based oxyhalides such as $PbBiO_2Cl$ and $PbBi_3O_4Cl_3$.[20,39] Additionally, $PbVO_3Cl$ shows a distinct contribution from Cl-3p orbitals. The CBMs of all compounds are primarily composed of V-3d orbitals, with additional contributions from O-2p and Pb-6p orbitals. These results suggest that the more positive CBMs of Pb–V oxyhalides than that of conventional oxyhalide photocatalysts can be attributed to the introduction of the V^{5+} cation, which has a high ionization energy. Furthermore, the most positive CBM of $PbVO_3Cl$ consists almost entirely of V orbitals with a small contribution from O orbitals. This indicates that the variation in CBM positions among Pb–V oxyhalides arises not from changes in the orbital composition forming the CBM but from differences in the energy of the V-3d orbitals themselves.

P. A. Cox previously illustrated how bands in extended solids are formed from isolated atoms (Fig. S9†).[40] The band structures can be determined by considering the following factors: (1) the electron affinity of anions or the ionization potential of cations, (2) the Madelung potential at each crystallographic site, (3) polarization effects, and (4) the bandwidth arising from orbital hybridizations. As discussed above, in the case of the Pb–V oxyhalide system, the energy levels of the V orbitals at crystallographic sites appear to play a significant role in determining the CBM positions. Fig. 5d shows the Madelung site potential of
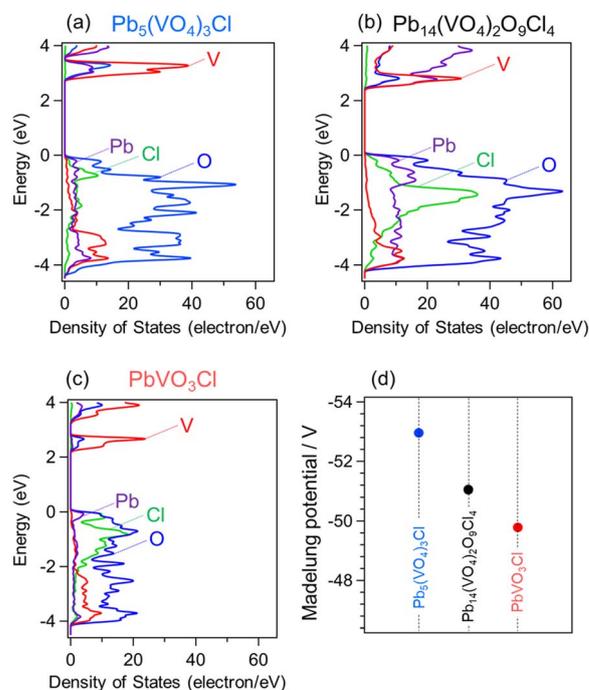

Fig. 4 Band diagrams of Pb–V-based oxyhalides, along with those of conventional oxyhalide photocatalysts. The band levels of Bi_4NbO_8Cl and $PbBiO_2Cl$ were referred from previous studies.[19,20]

Fig. 5 (a–c) Partial density of states of $Pb_5(VO_4)_3Cl$, $Pb_{14}(VO_4)_2O_9Cl_4$, and $PbVO_3Cl$. (d) Madelung site potentials of vanadium in the Pb–V-based oxyhalides.

This journal is © The Royal Society of Chemistry 2025

J. Mater. Chem. A, 2025, **13**, 25356–25362 | **25359**

vanadium in each Pb–V oxyhalide. These values are significantly influenced by the crystal structures, and their sequence aligns closely with the CBM positions of the Pb–V oxyhalides. This correlation strongly suggests that the most positive Madelung site potential for V in $PbVO_3Cl$ substantially stabilizes its orbitals, resulting in the most positive CBM among that of the materials studied.

Photocatalytic O_2 evolution

The Pb–V oxyhalides possess appropriate band levels suitable for reducing $Fe^{3+}(E^0(Fe^{3+}/Fe^{2+}) = 0.77$ V *vs.* NHE) and oxidizing water to O_2. The O_2 evolution activities of the three Pb–V oxyhalides were evaluated using Fe^{3+} as an electron acceptor under visible light irradiation. The $(Fe,Ru)O_x$ cocatalyst was loaded to enhance the O_2 evolution rate (Fig. S10†), as is often done with oxyhalide photocatalysts functioning as an OEP in Z-scheme systems with Fe^{3+}/Fe^{2+} redox mediators.[36] Fig. 6a shows the time course of O_2 evolution. Among the three oxyhalides, only $PbVO_3Cl$ exhibited O_2 evolution activity under visible light, while $Pb_5(VO_4)_3Cl$ and $Pb_{14}(VO_4)_2O_9Cl_4$ showed negligible activity. A similar trend was observed in the photocurrent response measurements (Fig. S11†). The XRD pattern of $PbVO_3Cl$ after the O_2 evolution reaction revealed almost no changes compared to that of pristine $PbVO_3Cl$, confirming that $PbVO_3Cl$ functioned stably as an OEP (Fig. S12†). The significantly higher O_2 evolution activity of $PbVO_3Cl$ compared to other Pb–V oxyhalides can be attributed to two main factors: (1) the broader visible light absorption up to the longest

wavelengths among the Pb–V oxyhalides as seen in Fig. 3a, and (2) the superior charge carrier transport properties. The second factor was evaluated using time-resolved microwave conductivity (TRMC) measurements,[41–43] wherein the intensity of TRMC signals on oxyhalides (*e.g.*, Bi_4TaO_8Cl and $PbBiO_2Cl$) has been proven to strongly correlate with their photocatalytic activity.[44,45] Fig. 6b shows the TRMC kinetics for each oxyhalide. $PbVO_3Cl$ exhibited the highest photoconductivity $(\varphi\Sigma\mu)$ signal among the three oxyhalides. Fig. 6c highlights the structural features (VO_4 or VO_5 units) underlying this property. The VO_4 units in $Pb_5(VO_4)_3Cl$ and $Pb_{14}(VO_4)_2O_9Cl_4$ are isolated, while the VO_5 units in $PbVO_3Cl$ are interconnected through edge-sharing. This interconnected feature facilitates superior electron transport, resulting in a higher TRMC signal. These findings reveal that the differences in crystal structures of Pb–V-based oxyhalides critically influence their light absorption and charge carrier transport properties, playing a crucial role in determining their photocatalytic activity.

Z-scheme water-splitting

Finally, visible-light-driven Z-scheme water-splitting was attempted using $PbVO_3Cl$ as the OEP. The schematic image is illustrated in Fig. S13.† Before constructing the system, various Fe^{3+} species with different counter anions were tested to identify the optimal precursor of the Fe^{3+}/Fe^{2+} redox mediator (Fig. 7a). The results revealed that $Fe(NO_3)_3$ and $Fe(ClO_4)_3$ were the most suitable, likely due to differences in the state of Fe aqua complexes, as suggested previously.[46] Similar trends were also observed with other oxyhalides, such as $PbBiO_2Cl$.[20] Subsequently, Z-scheme water-splitting was attempted using $SrTiO_3$:Rh as the HEP and $Fe(ClO_4)_3$ (or $Fe(NO_3)_3$) as the Fe^{3+}/Fe^{2+} redox mediator. When $Fe(NO_3)_3$ was used, gas production rates were very low, and H_2 and O_2 were not generated in a stoichiometric ratio $(2:1)$ (Fig. S14†). In contrast, using $Fe(ClO_4)_3$ led to the relatively steady evolution of H_2 and O_2 in a $2:1$ stoichiometric ratio, confirming successful Z-scheme water splitting under visible light (Fig. 7b). Since the O_2 evolution activity of $PbVO_3Cl$ was comparable when using either $Fe(ClO_4)_3$ or $Fe(NO_3)_3$, the differences in gas evolution rates in
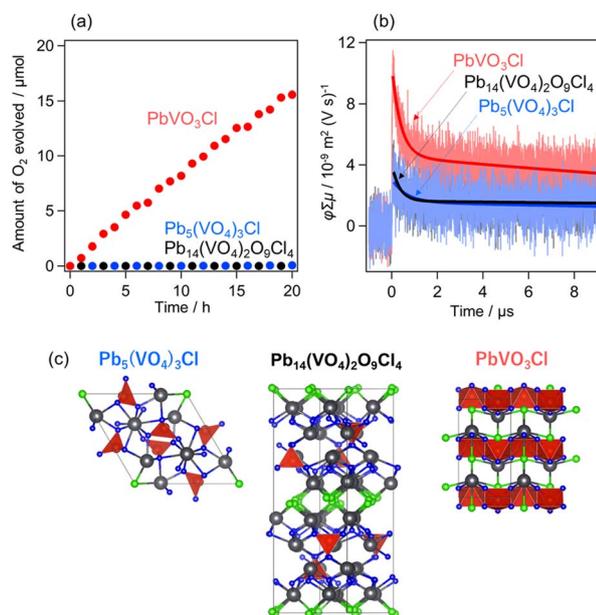

Fig. 6 (a) Photocatalytic O_2 evolution using $Pb_5(VO_4)_3Cl$, $Pb_{14}(VO_4)_2O_9Cl_4$, and $PbVO_3Cl$ in aqueous $Fe(NO_3)_3$ solution (5 mM, 250 mL, pH 2.4) under visible light irradiation ($\lambda > 400$ nm). $(Fe,Ru)O_x$ was loaded as a cocatalyst. (b) TRMC transients $(\varphi\Sigma\mu)$ of $Pb_5(VO_4)_3Cl$, $Pb_{14}(VO_4)_2O_9Cl_4$, and $PbVO_3Cl$ after excitation at 355 nm. The solid line represents the curve obtained through double-exponential fitting. (c) Crystal structures highlight each material's VO_4 or VO_5 units.
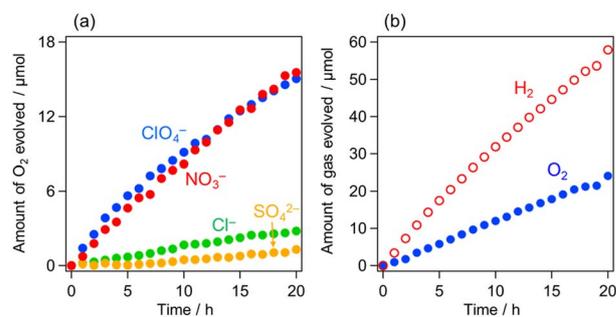

Fig. 7 (a) O_2 evolution over $(Fe,Ru)O_x/PbVO_3Cl$ from an aqueous Fe^{3+} solution (5 mM, 250 mL) with different counter anions (ClO_4^-, NO_3^-, Cl^-, or SO_4^{2-}) under visible-light irradiation ($\lambda > 400$ nm). (b) Z-scheme water splitting using $(Fe,Ru)O_x/PbVO_3Cl$ as an OEP and $Ru/SrTiO_3$:Rh as a HEP under visible light ($\lambda > 400$ nm) in an aqueous $Fe(ClO_4)_3$ solution (5 mM, 250 mL, pH 2.4).

25360 | *J. Mater. Chem. A*, 2025, **13**, 25356–25362

This journal is © The Royal Society of Chemistry 2025

the Z-scheme are likely attributed to the counter anion-dependent H_2 evolution activity of $SrTiO_3$:Rh.[47] Notably, even when unmodified $PbVO_3Cl$ (*i.e.* without $(Fe,Ru)O_x$ loading) was employed as the OEP, Z-scheme water splitting still proceeded, although the activity was moderately reduced (Fig. S15†). In conclusion, visible-light-driven Z-scheme water splitting was achieved for the first time using a V-based oxyhalide ($PbVO_3Cl$) as an OEP.

Conclusions

We demonstrated the potential of V-based oxyhalides as OEPs in Z-scheme water-splitting systems. The Pb–V-based oxyhalides exhibited more positive CBMs compared to conventional oxyhalide photocatalysts, with $PbVO_3Cl$ showing the most positive CBM and the smallest band gap among the investigated Pb–V oxyhalides, attributed to the more positive Madelung site potential of vanadium. $PbVO_3Cl$ features a unique structure with interconnected VO_5 units, significantly enhancing its carrier transport properties. The smaller band gap and superior carrier transport properties of $PbVO_3Cl$ enabled it to function as the first V-based oxyhalide OEP in a Z-scheme water-splitting system. While $PbVO_3Cl$ exhibits an ideal CBM position, its VBM remains excessively deep (positive), limiting its overall efficiency. The combination of vanadium introduction and valence band engineering could further narrow the band gap. Similar conduction band engineering could be achieved by introducing cations with high ionization energies other than vanadium.

Data availability

The data supporting this article have been included as part of the ESI.†

Conflicts of interest

There are no conflicts to declare.

Acknowledgements

Notes and references

1 A. Fujishima and K. Honda, *Nature*, 1972, **238**, 37–38.
2 A. J. Bard, *Science*, 1980, **207**, 139–144.
3 K. Domen, J. N. Kondo, M. Hara and T. Takata, *Bull. Chem. Soc. Jpn.*, 2000, **73**, 1307–1331.
4 A. Kudo and Y. Miseki, *Chem. Soc. Rev.*, 2009, **38**, 253–278.
5 R. Abe, *J. Photochem. Photobiol., C*, 2010, **11**, 179–209.
6 K. Maeda, *J. Photochem. Photobiol., C*, 2011, **12**, 237–268.
7 F. E. Osterloh, *Chem. Soc. Rev.*, 2013, **42**, 2294–2320.
8 S. S. Chen, T. Takata and K. Domen, *Nat. Rev. Mater.*, 2017, **2**, 17050.
9 K. Sayama, K. Mukasa, R. Abe, Y. Abe and H. Arakawa, *Chem. Commun.*, 2001, **23**, 2416–2417.
10 K. Maeda, *ACS Catal.*, 2013, **3**, 1486–1503.
11 T. Hisatomi, J. Kubota and K. Domen, *Chem. Soc. Rev.*, 2014, **43**, 7520–7535.
12 Y. O. Wang, H. Suzuki, J. J. Xie, O. Tomita, D. J. Martin, M. Higashi, D. Kong, R. Abe and J. W. Tang, *Chem. Rev.*, 2018, **118**, 5201–5241.
13 W. Zhao, K. Maeda, F. X. Zhang, T. Hisatomi and K. Domen, *Phys. Chem. Chem. Phys.*, 2014, **16**, 12051–12056.
14 T. Kato, Y. Hakari, S. Ikeda, Q. X. Jia, A. Iwase and A. Kudo, *J. Phys. Chem. Lett.*, 2015, **6**, 1042–1047.
15 R. Abe, T. Takata, H. Sugihara and K. Domen, *Chem. Commun.*, 2005, **30**, 3829–3831.
16 M. Higashi, R. Abe, T. Takata and K. Domen, *Chem. Mater.*, 2009, **21**, 1543–1549.
17 D. J. Martin, P. J. T. Reardon, S. J. A. Moniz and J. W. Tang, *J. Am. Chem. Soc.*, 2014, **136**, 12568–12571.
18 R. Abe, K. Shinmei, N. Koumura, K. Hara and B. Ohtani, *J. Am. Chem. Soc.*, 2013, **135**, 16872–16884.
19 H. Fujito, H. Kunioku, D. Kato, H. Suzuki, M. Higashi, H. Kageyama and R. Abe, *J. Am. Chem. Soc.*, 2016, **138**, 2082–2085.
20 H. Suzuki, H. Kunioku, M. Higashi, O. Tomita, D. Kato, H. Kageyama and R. Abe, *Chem. Mater.*, 2018, **30**, 5862–5869.
21 D. Kato, H. Suzuki, R. Abe and H. Kageyama, *Chem. Sci.*, 2024, **15**, 11719–11736.
22 H. Kunioku, M. Higashi, O. Tomita, M. Yabuuchi, D. Kato, H. Fujito, H. Kageyama and R. Abe, *J. Mater. Chem. A*, 2018, **6**, 3100–3107.
23 D. Kato, K. Hongo, R. Maezono, M. Higashi, H. Kunioku, M. Yabuuchi, H. Suzuki, H. Okajima, C. C. Zhong, K. Nakano, R. Abe and H. Kageyama, *J. Am. Chem. Soc.*, 2017, **139**, 18725–18731.
24 K. Ogawa, R. Sakamoto, C. C. Zhong, H. Suzuki, K. Kato, O. Tomita, K. Nakashima, A. Yamakata, T. Tachikawa, A. Saeki, H. Kageyama and R. Abe, *Chem. Sci.*, 2022, **13**, 3118–3128.
25 K. Ogawa, H. Suzuki, C. C. Zhong, R. Sakamoto, O. Tomita, A. Saeki, H. Kageyama and R. Abe, *J. Am. Chem. Soc.*, 2021, **143**, 8446–8453.
26 D. Ozaki, H. Suzuki, K. Ogawa, R. Sakamoto, Y. Inaguma, K. Nakashima, O. Tomita, H. Kageyama and R. Abe, *J. Mater. Chem. A*, 2021, **9**, 8332–8340.
27 H. Kunioku, M. Higashi, C. Tassel, D. Kato, O. Tomita, H. Kageyama and R. Abe, *Chem. Lett.*, 2017, **46**, 583–586.
28 A. Sahin and M. Emirdag-Eanes, *Z. Kristallogr. - New Cryst. Struct.*, 2007, **222**, 159–160.
29 J. B. Trotter and W. H. Barnes, *Can. Mineral.*, 1958, **6**, 161–173.

This journal is © The Royal Society of Chemistry 2025

J. Mater. Chem. A, 2025, **13**, 25356–25362 | **25361**

30 M. Cooper and F. C. Hawthorne, *Am. Mineral.*, 1994, **79**, 550–554.

31 U. Dang, W. Zaheer, W. Zhou, A. Kandel, M. Orr, R. W. Schwenz, G. Laurita, S. Banerjee and R. T. Macaluso, *Chem. Mater.*, 2020, **32**, 7404–7412.

32 M. Nakamura, K. Oqmhula, K. Utimula, M. Eguchi, K. Oka, K. Hongo, R. Maezono and K. Maeda, *Chem.–Asian J.*, 2020, **15**, 540–545.

33 V. Petricek, M. Dusek and L. Palatinus, *Z. Kristallogr. - Cryst. Mater.*, 2014, **229**, 345–352.

34 K. Momma and F. Izumi, *J. Appl. Crystallogr.*, 2011, **44**, 1272–1276.

35 S. J. Clark, M. D. Segall, C. J. Pickard, P. J. Hasnip, M. I. J. Probert, K. Refson and M. C. Payne, *Z. Kristallogr.*, 2005, **220**, 567–570.

36 A. Nakada, H. Suzuki, J. J. M. Verizo, K. Ogawa, M. Higashi, A. Saeki, A. Yamakata, H. Kageyama and R. Abe, *ACS Appl. Mater. Interfaces*, 2019, **11**, 45606–45611.

37 R. Konta, T. Ishii, H. Kato and A. Kudo, *J. Phys. Chem. B*, 2004, **108**, 8992–8995.

38 Y. Sasaki, A. Iwase, H. Kato and A. Kudo, *J. Catal.*, 2008, **259**, 133–137.

39 H. Suzuki, M. Higashi, O. Tomita, Y. Ishii, T. Yamamoto, D. Kato, T. Kotani, D. Ozaki, S. Nozawa, K. Nakashima, K. Fujita, A. Saeki, H. Kageyama and R. Abe, *Chem. Mater.*, 2021, **33**, 9580–9587.

40 P. A. Cox, *The Electronic Structure and Chemistry of Solids*, Oxford Science Publications, Oxford, 1986, p. 146.

41 A. Saeki, S. Yoshikawa, M. Tsuji, Y. Koizumi, M. Ide, C. Vijayakumar and S. Seki, *J. Am. Chem. Soc.*, 2012, **134**, 19035–19042.

42 A. Saeki, M. Tsuji and S. Seki, *Adv. Energy Mater.*, 2011, **1**, 661–669.

43 A. Saeki, Y. Koizumi, T. Aida and S. Seki, *Acc. Chem. Res.*, 2012, **45**, 1193–1202.

44 H. Suzuki, M. Higashi, H. Kunioku, R. Abe and A. Saeki, *ACS Energy Lett.*, 2019, **4**, 1572–1578.

45 H. Suzuki, S. Kanno, M. Hada, R. Abe and A. Saeki, *Chem. Mater.*, 2020, **32**, 4166–4173.

46 Y. Miseki, H. Kusama, H. Sugihara and K. Sayama, *Chem. Lett.*, 2010, **39**, 846–847.

47 H. Kato, Y. Sasaki, A. Iwase and A. Kudo, *Bull. Chem. Soc. Jpn.*, 2007, **80**, 2457–2464.

25362 | *J. Mater. Chem. A*, 2025, **13**, 25356–25362

This journal is © The Royal Society of Chemistry 2025